Journal Européen des Systèmes Automatisés
Vol.59, No. 7, July, 2026, pp. 1893-1902
Journal homepage: http://iieta.org/journals/jesa

Optimized FS-MPC Control of a PMSG-Based Wind Energy System in Grid-Connected Low-Energy Buildings

Abdelaali Alibi[1*], Drid Said[2], Laarbi Chrifi Alaoui[3], Tahar Bahi[4]

[1] Electrical Engineering Department, Laboratory LSPIE, University of Batna2, Batna 05001, Algeria
[2] Higher National School of Renewable Energies, Environment and Sustainable Development, Batna 05078, Algeria
[3] Laboratory of Innovative Technology (LTI), University of Picardie Jules Verne, IUT of Cuffies, 02880, France
[4] LASA Laboratory, Badji Mokhtar-Annaba University, Annaba 23000, Algeria

Corresponding Author Email: a.alibi@univ-batna2.dz

https://doi.org/10.18280/jesa.590707

Received: 1 December 2025
Revised: 1 July 2026
Accepted: 10 July 2026
Available online: 31 July 2026

Keywords:
wind energy conversion systems, finite-state model predictive control, positive-energy building, permanent magnet synchronous generator, turbine Maximum Power Point Tracking, power quality

ABSTRACT

This paper proposes a finite-state model predictive control (FS-MPC) strategy for the control of a permanent magnet synchronous generator (PMSG)-based wind energy conversion system. The proposed system is designed to meet the electricity demand of a building coupled to both the wind energy conversion systems (WECS) and the distribution grid. The fundamental aim is to alleviate stress on the grid and reduce its contribution to the building's power supply. First, the mathematical modelling of the system components is developed, followed by the development of a predictive model equation used to regulate the generated power and optimize the converter switching states. The suggested control approach leverages the discrete characteristic of power converters to predict the future evolution of output currents. Subsequently, the ideal voltage vector, minimizing a predefined cost function, is retained and applied at each sampling time. A key advantage of this approach, when applied to both converters, is its ability to control them simultaneously through a unified cost function. The effectiveness and robustness of the proposed method against load and wind speed variations are validated through the simulation results. Its superiority is further validated by its accurate reference tracking, fast dynamic response, and high-quality current waveforms, particularly in terms of total harmonic distortion (THD) reduction.

1. INTRODUCTION

With the rise in oil prices, the environmental impact of electricity generation from fossil fuels, and the long-term risk of resource depletion, the global energy transition necessitates the development of clean, renewable, and inexhaustible energy sources. The Directive 2010/31/EU of the European Union of May 19, 2010, on the "Building Energy Performance" mandates that by December 31, 2020, all future buildings are expected to meet nearly zero energy consumption [1].

The application of renewable energy systems in residential buildings, whether isolated or grid-connected, is emerging as a key solution to reducing dependence on conventional power systems. These buildings can meet their own energy demands while injecting excess power into the grid, thereby transforming it into a vast gathering of decentralized renewable sources of energy.

Wind energy plays a significant role as a clean and sustainable power source. Generally, wind energy conversion systems (WECS) utilize either a doubly-fed induction generator (DFIG) or a permanent magnet synchronous generator (PMSG). The WECS-based PMSG offers several advantages over its DFIG counterpart [2, 3]. PMSG exhibits power losses approximately 35% lower than those of DFIG, along with higher efficiency, increased power density, and improved grid compatibility [4-6]. A key characteristic of PMSG is its operation at low rotor speed, making it particularly suitable for small-scale WECS. Since it does not require a gearbox, it is attached directly to the wind turbine shaft, reducing mechanical losses and maintenance requirements. The windings of the generator's stator are linked to both the building and the grid at the common connection point via a three-phase back-to-back converter, which regulates both the PMSG-side and grid-side operation. The DC-link consists of a shunt capacitor, which serves to interface the two converters, as illustrated by Figure 1.

The energy extracted from a wind turbine primarily depends on wind speed, as its nonlinear characteristics result in limited power output and low efficiency at varying speeds. To ensure maximum power extraction, several Maximum Power Point Tracking (MPPT) algorithms have been proposed [7-10]. Common techniques include P&O (Perturb and Observe) control and fuzzy logic-based MPPT, which operates without wind speed measurement. However, these methods exhibit undesirable oscillations around the MPP. When the turbine characteristics are well known, the tip-speed ratio (TSR) control is often preferred due to its simplicity and effectiveness in tracking the optimal rotor speed corresponding to the

Maximum Power Point (MPP) [11, 12]. The produced energy on the PMSG side is then efficiently transferred to both the building and the grid via the converter on the grid side.

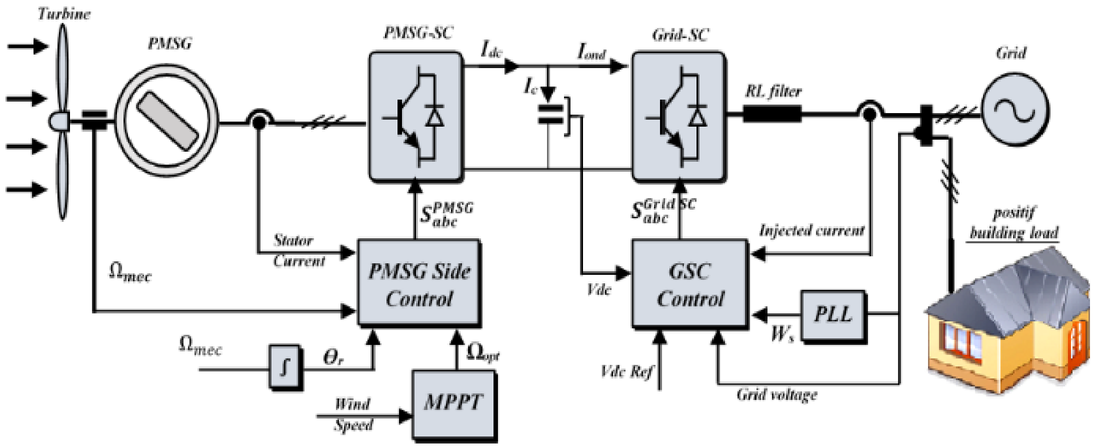

Figure 1. Wind energy conversion system configuration

The literature highlights various control strategies to regulate the back-to-back converter and achieve optimal WECS performance. Among these, Voltage Oriented Control (VOC) and Field Oriented Control (FOC) are widely used to implement MPPT algorithms by regulating PMSG rotor speed [13-15]. These techniques rely on PI controllers, which offer good steady-state performance but require nonlinear compensation to decouple the controlled currents. This compensation increases the sensitivity to parameter variations in the system. Direct torque control (DTC) is a widely used method for PMSG-side converter control, optimizing turbine power extraction while ensuring a fast and stable dynamic response. However, this technique requires high switching frequencies to minimize current and torque ripples [16, 17]. The back-stepping control method, proposed in the study [18], introduces a nonlinear control strategy for both PMSG- and grid-side converter (GSC), offering high accuracy, robustness, and fast transient response. However, its major drawback lies in the complexity introduced by repeated differentiation of nonlinear functions. Sliding Mode Control (SMC) has also been employed for back-to-back converter control, demonstrating robust performance against system uncertainties and wind speed variations [19, 20]. However, its main drawback is the steady-state chattering phenomenon. To overcome these limitations, researchers in the study [21] proposed an advanced finite-state model predictive control (FS-MPC) technique for grid-tied WECS. In their work, FS-MPC was applied separately to the PMSG-side converter (to maintain the turbine at MPP) and the GSC (to manage efficient power feed into the grid). The simulation results validated FS-MPC's effectiveness, demonstrating high current tracking accuracy and resilience to wind speed fluctuations. However, their study did not consider a grid-connected load, nor did it examine the impact of load variations on PMSG and grid power control.

FS-MPC has been recognized as a powerful approach for power converter control for its ability to consider the system's discrete nature, enabling accurate predictive models for controlled parameters. Its flexibility and robustness make it an attractive solution for WECS applications [22, 23].

This work focuses on the implementation of FS-MPC in a WECS supplying a positive-energy building connected to the grid. FS-MPC is introduced as a replacement for conventional PWM-based techniques and inner current control loops in both back-to-back converters. To achieve optimal performance, two separate cost functions will be employed for each converter to minimize system tracking errors. Additionally, we propose a unified cost function that simultaneously regulates both converters, offering a globally coordinated control strategy. The proposed controller and obtained results will prove the simplicity and superior performance of this technique relative to conventional approaches.

This paper is outlined as follows: In Section 2, we present the structure of the proposed WECS. Section 3 details the mathematical models of the wind turbine, PMSG, and system converters. In Section 4, we introduce the control strategy for both parts of the WECS. Section 5 is dedicated to the FS-MPC control theory, where we develop its application to both converters. The results of simulation under multiple operating modes of the proposed control method are illustrated in Section 6. Finally, conclusions are given in Section 7.

2. STRUCTURE OF THE WIND ENERGY SYSTEM

The considered system involves a PMSG driven by a wind turbine, a synchronous generator-side converter (PMSG-SC) used to control its speed to extract the maximum available kinetic power from the wind, and a GSC that connects the PMSG to both the building and the distribution grid through a back-to-back converter. The GSC ensures that the building's energy demand is met while injecting any excess power into the distribution grid. The overall structure of this system is illustrated in Figure 1.

3. SYSTEM MODELLING

3.1 Turbine model

A wind turbine converts the kinetic energy of the air stream crossing its swept area S into mechanical energy on the turbine shaft. The extractable power is always lower than the theoretical wind potential and depends mainly on the wind speed V and blade radius R, as expressed in Eq. (1).

$$P_m = \frac{1}{2} C_p(\lambda,\beta)\rho S V^3 \tag{1}$$

where, $S = \pi R^2$, R represents the blade length (m), ρ is the density of the air (kg/m^3), $C_p(\lambda,\beta)$ is the power coefficient that describes the aerodynamic efficiency of the turbine.

Several numerical approximations have been developed for determining the C_p expression. The expression modelling the C_p for the conversion system turbine in this work is given as [24-26]:

$$C_p = 0.5176\left(\frac{116}{\lambda'} - 0.4\beta - 5\right)e^{\frac{-21}{\lambda'}} + 0.0036.\lambda \quad (2)$$

where, λ' is given by the following equation:

$$\frac{1}{\lambda'} = \frac{1}{\lambda + 0.08\beta} - \frac{0.035}{\beta^2 + 1} \quad (3)$$

In this study, we assume a fixed pitch angle ($\beta = 0$) for various wind speed values. The turbine mechanical torque is derived from the turbine power Eq. (1) and is given by:

$$T_t = \frac{P_t}{\Omega_t} = \frac{0.5.C_p(\lambda,\beta).\rho.\pi.R^3\,V^2}{\lambda} \quad (4)$$

The turbine–generator dynamics are governed by the following differential equation:

$$J\frac{d\Omega_{mec}}{dt} = T_m - T_{em} - f\Omega_{mec} \quad (5)$$

where, T_{em} is the electromagnetic torque of the generator, $f = (f_t, f_{PMGS})$ and $J = (J_t, J_{PMSG})$ are respectively the inertia moment and the friction coefficient of turbine-generator system. Ω_{mec} is the PMSG rotor speed and $T_m = G.T_t$ is the torque on the shaft of the generator. Finally, G is the gearbox factor.

3.2 Modelling of the permanent magnet synchronous generator

The developed PMSG model is used to analyze its transient and steady-state performance. It also serves as a basis for defining its control laws [27].

The stator voltage equations (V_{sd}, V_{sq}) in the synchronous (d,q) frame are as follows:

$$\begin{cases} V_{sd} = R_s I_{sd} + \dfrac{d\emptyset_{sd}}{dt} - w_r\emptyset_{sq} \\ V_{sq} = R_s I_{sq} + \dfrac{d\emptyset_{sq}}{dt} + w_r\emptyset_{sd} \end{cases} \quad (6)$$

The flux equations are given as below:

$$\begin{cases} \emptyset_{sd} = L_{sd}I_{sd} + \emptyset_f \\ \emptyset_{sq} = L_{sq}I_{sq} \end{cases} \quad (7)$$

where, (I_{sd}, I_{sq}) and (L_d, L_q) represent the stator currents and inductances respectively, R_s resistor of the stator windings, ϕ_f is the magnetization flux and $w_r = p\Omega_{mec}$ electrical rotor speed, p is the pair pole number.

The electromagnetic torque delivered by the generator is given by:

$$T_{em} = \frac{3}{2}pI_{sq}\left[\phi_f + (L_d - L_q)I_{sd}\right] \quad (8)$$

3.3 Modelling of the grid side inverter and filter

The predictive current model of the GSC is derived from the coupling filter dynamics, expressed in the (α-β) reference frame by the following equations [12, 21]:

$$\frac{dI_{gr}^{\alpha}}{dt} = \frac{1}{L_f}(V_{inv}^{\alpha} - V_{gr}^{\alpha} - R_f I_{gr}^{\alpha}) \quad (9)$$

$$\frac{dI_{gr}^{\beta}}{dt} = \frac{1}{L_f}(V_{inv}^{\beta} - V_{gr}^{\beta} - R_f I_{gr}^{\beta}) \quad (10)$$

where, R_f and L_f are the resistance and inductance of the link filter; V_{gr} is the voltage at the coupling point of both the grid and the building. I_{gr} and V_{inv} represents the delivered current of the GSC.

4. WIND ENERGY CONVERSION SYSTEM CONTROL STRATEGY

In this paper, the control system consists of two main control units:

PMSG-SC Control Unit: Regulates the turbine speed to ensure operation at the Maximum Power Point (MPP).

GSC Control Unit: Ensures DC-link voltage regulation to maintain Grid stability and controls the power exchange between the WECS, the load, and the grid.

The overall control architecture is designed to optimize energy conversion efficiency while ensuring system stability and reliability.

4.1 Turbine power maximization

Several strategies exist to extract the maximum available energy in the wind. Among them, the TSR technique, an MPPT technique based on speed control, determines the optimal turbine speed that maximizes the converted mechanical power by adjusting the electromagnetic torque of the PMSG, the only directly controllable input, as explained in Figure 1.

The reference speed for the optimal TSR 'λ_{opt}' is calculated using the following tip-speed expression [28, 29]:

$$\Omega_{opt} = \frac{\lambda_{opt}V}{R} \quad (11)$$

From Eq. (8), the electromagnetic torque 'T_{em}' depends on both the (d,q) axis of stator currents 'I_{sd}' and 'I_{sq}'. By setting the d-axis current 'I_{sd}' to zero, the torque expression is decoupled, allowing the reference torque to be controlled by the q-axis current [30, 31], as given by:

$$\begin{cases} I_{sd}^{Ref} = 0 \\ I_{sq}^{Ref} = \dfrac{2}{3.p.\emptyset_f}T_{em}^{Ref} \end{cases} \quad (12)$$

The overall operating model and MPPT-based power control strategy for the turbine are summarized in the block diagram shown in Figure 2.

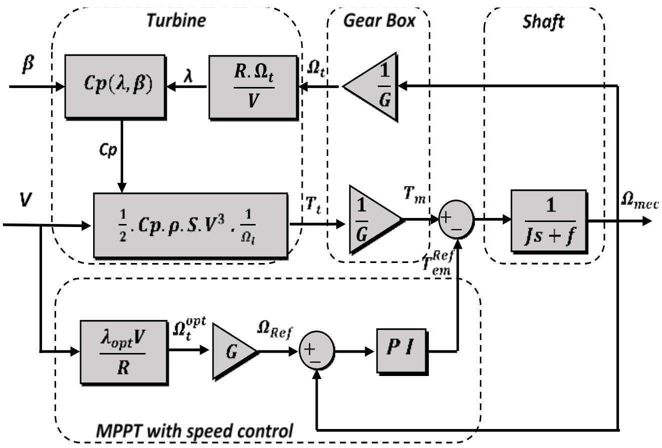

Figure 2. Turbine global model and Maximum Power Point Tracking (MPPT) power control

4.2 DC-link voltage regulation

Fluctuations in the DC-link voltage are a direct consequence of any energy disequilibrium within the DC-link capacitor. The control strategy ensures a balance between the power generated by the PMSG and the power provided to the building and grid. Eq. (13) describes the dynamics governing the DC-link voltage [11, 25, 26, 31].

$$\frac{dV_{DC}}{dt} = \frac{1}{c}\left(I_{DC}^{PMSG} - I_{DC}^{inv}\right) \tag{13}$$

The DC-link reference voltage V_{DC_Ref} is a critical parameter for the proper operation of the back-to-back converter. In this study, V_{DC_Ref} is selected to satisfy the controllability condition: $V_{DC\_Ref} > \sqrt{2} \times U_{g(L-L)}$, where $U_{gr(L-L)}$ represents the peak value of the grid voltage.

The grid side inverter reference current is provided by the PI regulator that regulates the DC-link voltage, as expressed in Eq. (14) [32].

$$I_{DC}^{PMSG} - I_{DC}^{inv} = \left(k_p + \frac{k_i}{s}\right).(V_{DC}^{Ref} - V_{DC}) \tag{14}$$

The DC-bus structure is illustrated in Figure 3, where I_{DC}^{PMSG} is the rectified current supplied by the PMSG-SC, I_{DC}^{inv} is the input current of the grid-side inverter, and k_p and k_i denote the PI controller parameters.

The DC-link PI controller parameters (k_p,k_i) were designed using the pole placement method to ensure precise closed-loop stability. By targeting a second-order response with a damping ratio of ζ = 0.707, the system achieves an optimal balance between fast settling time and minimal voltage overshoot.

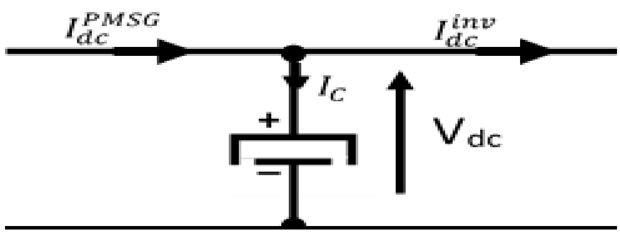

Figure 3. DC-link bus

5. FINITE-STATE MODEL PREDICTIVE CONTROL

FS-MPC takes advantage of the discrete switching character of power converters by predicting system responses for all admissible switching states and choosing the one that minimizes a specified cost function [33]. This method enables efficient converter control by predicting future system states based on the current evolution. The general FS-MPC structure is shown in Figure 4, where the system corresponds to either the PMSG or the building distribution grid.

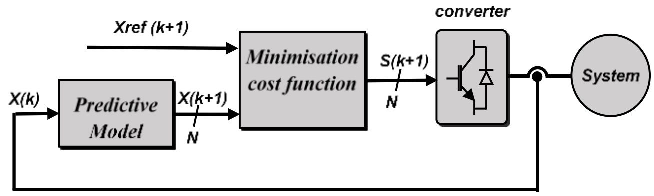

Figure 4. General diagram of the finite-state model predictive control (FS-MPC)

5.1 Generator-side predictive converter control

Figure 5 illustrates the predictive control scheme of the machine-side converter. At each sampling period, the controller determines the voltage vector that minimizes the tracking error between the stator current components I_{sd} and I_{sq} and their respective references in the (d, q) reference frame. For decoupled electromagnetic torque control, the d-axis current is set to zero. The reference on q-axis of the current I_{sq}^{Ref}, defined in Eq. (12), is generated by a PI regulator in the outer speed control loop of the PMSG.

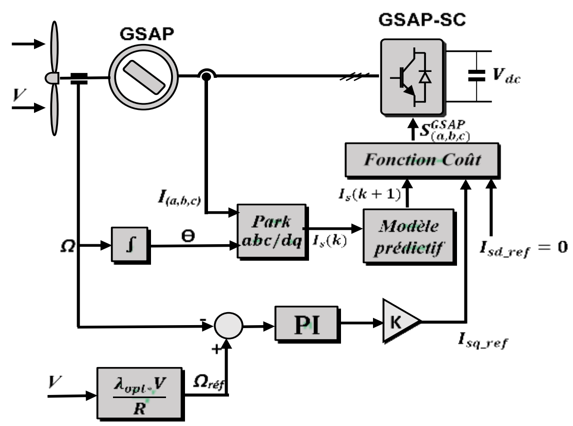

Figure 5. Block diagram of the machine-side converter predictive control

Based on Eqs. (7) and (8), the predictive model of the stator currents is derived as follows:

$$\frac{dI_{sd}}{dt} = \frac{1}{L_d}\left(V_{sd} - R_s I_{sd} + w_r L_q I_{sq}\right) \tag{15}$$

$$\frac{dI_{sq}}{dt} = \frac{1}{L_q}\left(V_{sq} - R_s I_{sq} + w_r L_d I_{sd} - w_r \phi_f\right) \tag{16}$$

The discretization of Eqs. (15) and (16) is carried out using the forward Euler process [12, 21]. The resulting discrete expressions used to predict the currents are given by:

$$I_{sd}(k+1) = \frac{T_s}{L_d} V_{sd}(k) + \left(1 - T_s \frac{R_s}{L_d}\right) I_{sd}(k) + \frac{T_s}{L_d} w_r(k) L_q I_{sq}(k) \quad (17)$$

$$I_{sq}(k+1) = \frac{T_s}{L_q} V_{sq}(k) + \left(1 - T_s \frac{R_s}{L_q}\right) I_{sq}(k) + \frac{T_s}{L_q} w_r(k) L_d I_{sd}(k) + \frac{T_s}{L_q} w_r(k) \phi_f) \quad (18)$$

Here, T_s denotes the sampling time, $[I_{sd}(k), I_{sq}(k)]$ are the currents measured at the instant k, and $[I_{sd}(k+1), I_{sq}(k+1)]$ are the predicted currents for instant k + 1. These predictions depend on the voltage vector $V_{s(d,q)}(k)$ applied by the converter during the kth interval. The components V_{sd} and V_{sq} in the d-q frame are obtained through the following coordinate transformation [34]:

$$V_{s(d,q)}(k) = V_{s(\alpha,\beta)}(k). e^{-j\theta(k)} \quad (19)$$

where, $V_{s\alpha}$ and $V_{s\beta}$ are the voltage converter voltage components in the (α, β) frame, corresponding to the eight possible switching states registered in Table 1.

Table 1. Possible switching states

$S_a^{PMSG,GS}$	$S_b^{PMSG,GS}$	$S_c^{PMSG,GS}$	$V_{s\alpha}$	$V_{s\beta}$
0	0	0	0	0
1	0	0	$2V_{DC}/3$	0
1	1	0	$V_{DC}/3$	$V_{DC}/\sqrt{3}$
0	1	0	$-V_{DC}/3$	$V_{DC}/\sqrt{3}$
0	1	1	$-2V_{DC}/3$	0
0	0	1	$-V_{DC}/3$	$-V_{DC}/\sqrt{3}$
1	0	1	$V_{DC}/3$	$-V_{DC}/\sqrt{3}$
1	1	1	0	0

The error between the predicted currents $I_{s(d,q)}(k+1)$ and the reference currents $I_{s(d,q)}^{Ref}(k)$ in the d-q frame are evaluated using the following equations:

$$\begin{cases} \Delta I_{sd}(k+1) = |I_{sd}(k+1) - I_{sd}^{Ref}(k)| \\ \Delta I_{sq}(k+1) = |I_{sq}(k+1) - I_{sq}^{Ref}(k)| \end{cases} \quad (20)$$

$I_{sd}^{Ref}(k), I_{sq}^{Ref}(k)$ are the reference currents determined by Eq. (12).

The cost function to be minimized is defined as the sum of the squared errors:

$$Cost_{PMSG} = (\Delta I_{sd}(k+1))^2 + (\Delta I_{sq}(k+1))^2 \quad (21)$$

The optimal switching combination is then selected as the one corresponding to the minimum cost function value.

5.2 Grid side predictive converter control

The primary function of the GSC control is to ensure that all generated energy is effectively used to meet the building's demand, with any surplus injected into the grid. This requires satisfying several constraints, including matching the load, maintaining grid stability, and delivering high-quality power. The reference current magnitude is determined by the outer DC voltage regulation loop given by the following equation [23].

$$I_{gr\ Ref}^{max} = \frac{\sqrt{2}\, V_{DCRef}}{3\, V_s} I_{DC}^{inv} \quad (22)$$

A phase-locked loop (PLL) is employed to ensure synchronization of this current ($I_{g\ Ref}^{max}$) with the grid frequency. The control scheme is given by Figure 6.

We proceed with the same procedure as with the machine-side converter control. Using a forward Euler approximation, the discretized current prediction equations are given by the following equations [12, 21]:

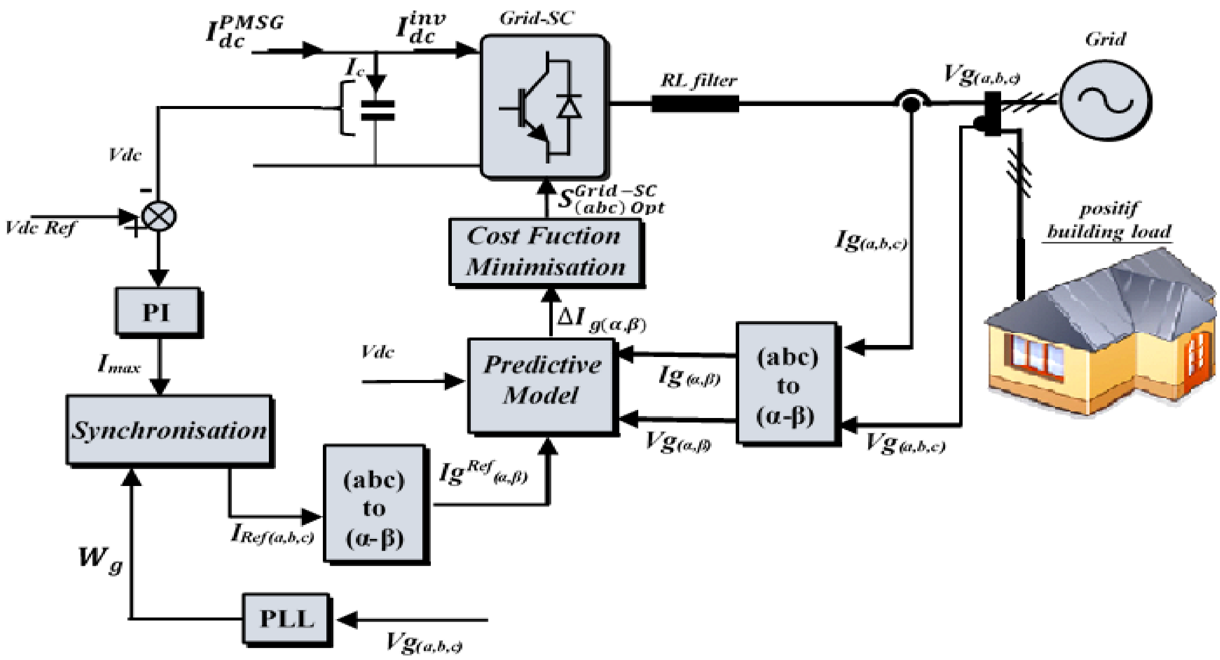

Figure 6. Model predictive control scheme of the grid-side converter (GSC)

$$I_{gr}^{\alpha}(k+1) = \left(1 - T_s \frac{R_f}{L_f}\right) I_{gr}^{\alpha}(k) + T_s \frac{1}{L_f} V_{inv}^{\alpha}(k) - T_s \frac{1}{L_f} V_{gr}^{\alpha}(k) \quad (23)$$

$$I_{gr}^{\beta}(k+1) = \left(1 - T_s \frac{R_f}{L_f}\right) I_{gr}^{\beta}(k) + T_s \frac{1}{L_f} V_{inv}^{\beta}(k) - T_s \frac{1}{L_f} V_{gr}^{\beta}(k) \quad (24)$$

Here, $V_{gr}(k)$ represents the building-linked bus voltage during the k^{th} sampling time, I_{gr} (k) denotes the current measured at the k^{th} sampling instant, and $I_{gr}(k+1)$ is the current predicted for the following sampling period. Additionally, $V_{inv}(k)$ is the output inverter voltage in the (α-β) frame, which corresponds to the eight possible switching states summarized in the previous table.

In the same way, the cost function terms are defined as the squared errors between the predicted currents and their corresponding reference values, as expressed in Eqs. (25) and (26).

$$\begin{cases} \Delta I_{gr}^{\alpha}(k+1) = |I_{gr}^{\alpha}(k+1) - I_{grRef}^{\alpha}(k)| \\ \Delta I_{gr}^{\beta}(k+1) = |I_{gr}^{\beta}(k+1) - I_{grRef}^{\beta}(k)| \end{cases} \quad (25)$$

$$Cost_{inv} = \left(\Delta I_{gr}^{\alpha}(k+1)\right)^2 + \left(\Delta I_{gr}^{\beta}(k+1)\right)^2 \quad (26)$$

The optimal switching combination that minimizes this cost function is then selected and applied to the inverter.

5.3 Global optimized converter switching control

The proposed control strategy employs a unified cost function (Eq. (27)) to simultaneously coordinate the switching states of the machine-side and grid-side converters. Unlike decentralized MPC approaches where each converter is controlled by an independent cost function, the unified function ensures that the selection of the optimal voltage vector pair occurs within a single sampling interval Ts. This synchronization is crucial for the DC-link energy balance, as it allows the controller to anticipate the power flow exchange between the PMSG and the grid simultaneously.

The control scheme of the global model predictive control is given in Figure 7.

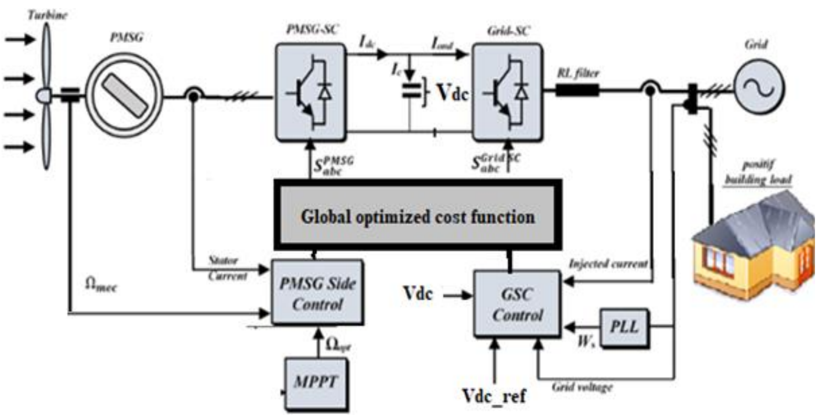

Figure 7. The proposed global control scheme

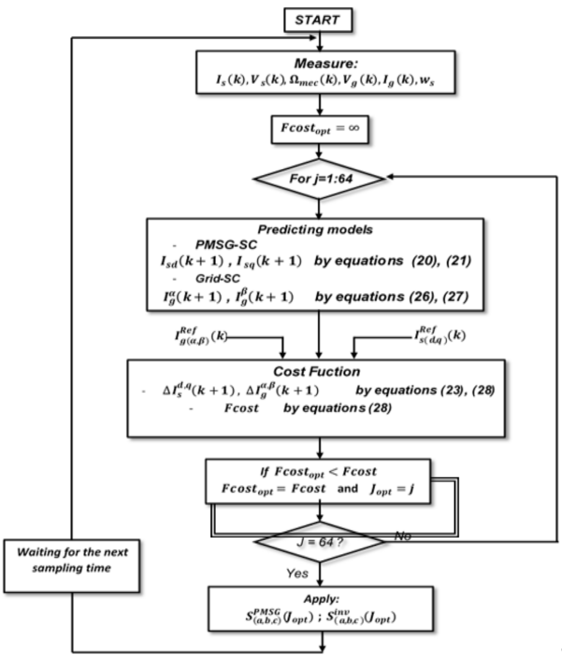

Figure 8. Flowchart of the global model predictive control

The overall proposed control flowchart is illustrated in Figure 8.

The global optimized cost function, which aggregates all error terms and criteria to be minimized, is defined as:

$$F_{cost} = Q_1.\left(\Delta I_{sd}(k+1)\right)^2 + Q_2.\left(\Delta I_{sq}(k+1)\right)^2 + Q_3.\left(\Delta I_{gr}^{\alpha}(k+1)\right)^2 + Q_4.\left(\Delta I_{gr}^{\beta}(k+1)\right)^2 + Q_5.Sw \quad (27)$$

In Eq. (27), the empirical weighting coefficients $Q_{i=1:5}$ are carefully selected to balance the individual terms in the cost function, ensuring its optimal minimization. Additionally, the term $'Sw'$ is included in the objective function to optimize the converter's switching and reduce power losses [30]. $'Sw'$ Is defined as follows:

$$Sw = \sum_{j=a,b,c} \left(\left|S_j^{PMSG}(k) - S_{jopt}^{PMSG}(k-1)\right| + \left|S_j^{inv}(k) - S_{jopt}^{inv}(k-1)\right| \right) \quad (28)$$

The selection of the weighting coefficients $(Q_1 - Q_5)$ is governed by a dynamic priority strategy based on the system's physical time constants. To ensure rapid transient response, the highest weights are allocated to the stator then the grid current components $(Q_1 - Q_4)$, which represent the fastest dynamics in the WECS.

6. SIMULATION RESULTS AND DISCUSSION

The WECS described in Figure 1 was simulated in a MATLAB-Simulink tool to evaluate the effectiveness of the proposed FS-MPC. Several scenarios, involving variations in both building load and wind speed, were considered, as illustrated in Figure 9.

Scenario 1: wind speed is below the cut-in speed (less than 3 m/s), while the building energy demand is at its peak value of 3 kW.

Scenario 2: wind speed rises from 3 m/s to 7 m/s between t = 1 s and t = 2 s.

Scenario 3: wind speed decreases to 6 m/s until t = 3 s, while maintaining a constant load of 3 kW.

Scenario 4: building load decreases to 2 kW while wind speed returns to 7 m/s.

The electric and mechanical data of the PMSG-based wind turbine, along with the grid and control parameters utilised in our study, are summarized in Table 2.

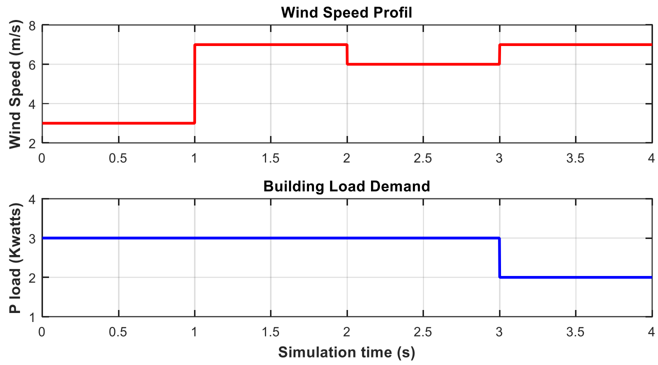

Figure 9. Wind speed and building load demand

Table 2. System parameters for simulation

Category	Parameter	Symbol	Value	Unit
Wind Turbine	Number of blades	n	3	
	Blade length (Radius)	R	3	m
	Moment of inertia	J_t	0.6	kg·m²
	Friction coefficient	f_t	0.01	
Permanent Magnet Synchronous Generator (PMSG)	Number of pole pairs	p	4	
	Stator resistance	R_s	0.895	Ω
	dq-axis inductances	L_d-L_q	0.0211-0.012	H
	Permanent magnet flux	Φ	0.6194	Wb
	Moment of inertia	J	0.00141	kg·m²
	Friction coefficient	f	0.001	
Grid & DC-Link	Grid Voltage / Frequency	V_g/f	230 / 50	V/Hz
	DC-link Capacitance	C	1000	uF
Control System	Sampling Parameter	T_s	1e-6	s
	DC-link PI controller	$(k_p$-$k_i)$	0.5-0.05	

Simulation results are presented in Figures 10-14 and in Table 3.

Table 3. Grid-side converter (GSC) current total harmonic distortion (THD)

Phase of Simulation	THD
Second mode of simulation Start time 1.2 s Number of cycles = 35	THD = 0.89%
Third mode of simulation Start time 2.2 s Number of cycles = 35	THD = 1.51%
Fourth mode of simulation Start time 3.2 s Number of cycles = 35	THD = 0.97%

Figure 10 shows the PMSG rotor speed and turbine power coefficient under various scenarios, while Figure 11 illustrates the machine currents in the (d-q) frame along with their reference values. Figure 12 depicts the controlled DC-link voltage, and Figure 13 provides details on the power for the PMSG, building load, and distribution grid. Additionally, Figure 14 offers a detailed view of the current and voltage evolution for one phase of the PMSG (Figure 14(A)), the distribution grid (Figure 14(B)), and the building load (Figure 14(C)), with focused plots across different simulation modes.

Finally, Table 3 summarizes the corresponding total harmonic distortion (THD) factor of the grid side converter current signals. Figure 11 demonstrates that the proposed control strategy effectively regulates the PMSG rotor speed, thereby maximizing the turbine power output. This performance is further validated by the turbine power coefficient C_p, which consistently remains at its optimal value ($C_p = 0.48$) across all simulation scenarios. Figure 12 illustrates that the controlled currents in the d-q frame accurately follow their reference values and remain decoupled, despite the inherent nonlinearities in the machine model that are not explicitly compensated by the control strategy.

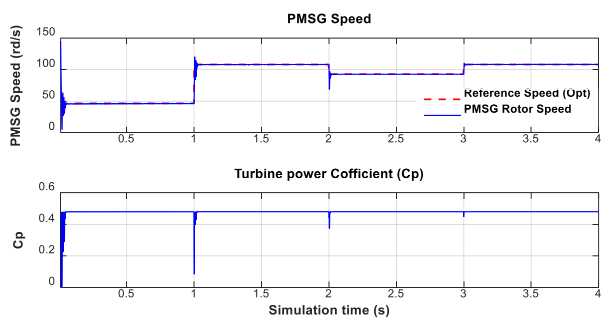

Figure 10. Permanent magnet synchronous generator (PMSG) speed and turbine power coefficient

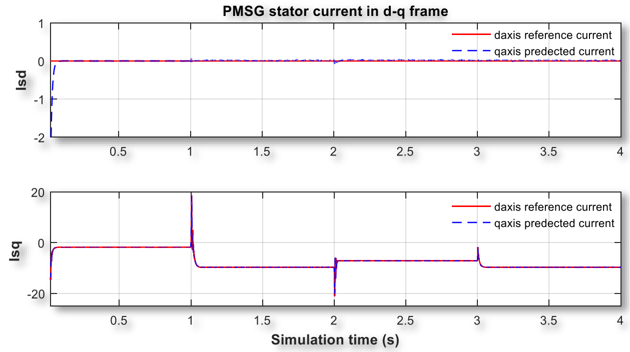

Figure 11. Permanent magnet synchronous generator (PMSG) stator control currents in d-q frame

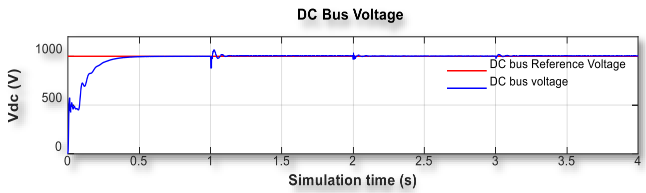

Figure 12. DC-link voltage control

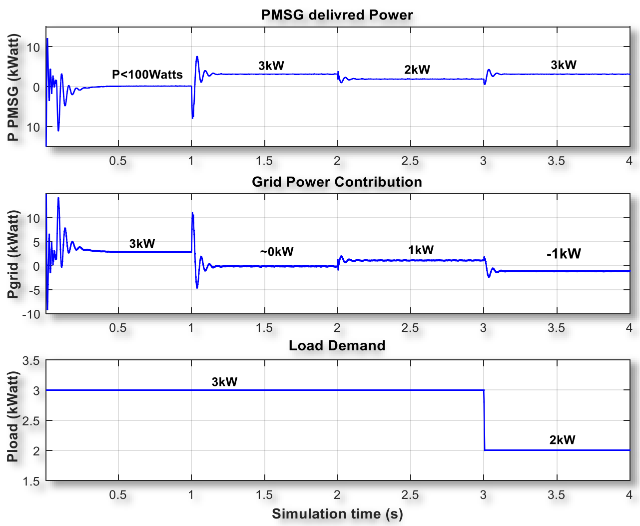

Figure 13. Different powers in the proposed wind energy conversion systems (WECS)

The results show that generator bootstrapping occurs only when wind speed surpasses 3 m/s. At lower wind speeds, the PMSG produces negligible power, and the building's energy demand is entirely supplied by the grid (Figures 13-14). When the average wind speed reaches approximately 7 m/s, the PMSG generates sufficient power to fully meet the building's electrical needs, reducing dependence on the grid. In cases where WECS output power decreases, the grid partially supplements the building's supply, as observed in the third scenario.

A building equipped with this WECS achieves positive energy when its production exceeds consumption. In the final simulation test, surplus energy is injected into the grid during low-demand periods, resulting in a grid current that becomes opposite in phase to the grid voltage (Figure 14 (B4)).

The results in Table 3 confirm the effectiveness of the proposed control strategy in providing high-quality energy to both the building and the grid. Even under the WECS's worst-case operating conditions, the THD remains below 1.5%.

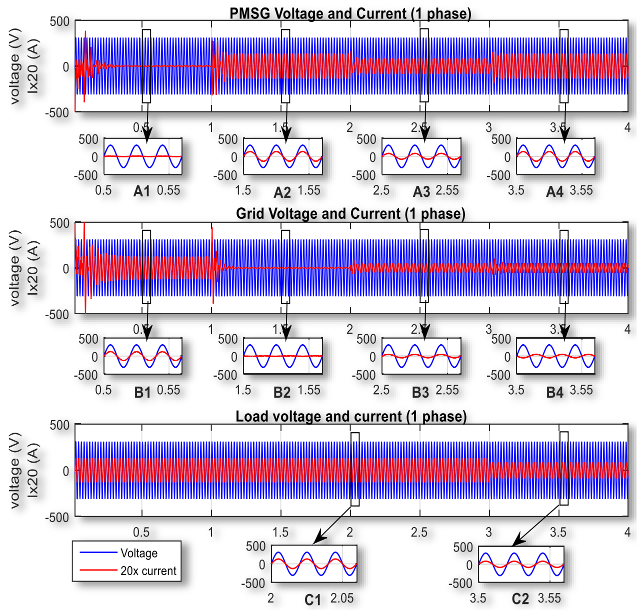

Figure 14. One-phase voltage and current of the wind energy conversion systems (WECS)

7. CONCLUSIONS

In this work, an FS-MPC strategy is applied to a PMSG-based WECS for powering a positive-energy building connected to the grid. The control technique is implemented on both the generator side and grid side converters to maximize energy utilization. On the generator side, FS-MPC extracts maximum power by correcting the electromagnetic torque to operate the turbine at its optimal speed. On the grid side, it optimizes power flow to meet the building's demand while injecting surplus energy into the distribution grid.

This controller, functioning as a modulation technique, is straightforward to implement and exploits the discrete nature of static converters to predict controlled variables at the next sampling instant. It avoids the need for linear regulators in the internal control loops, except for the outer DC-link voltage regulation and turbine speed control loops used in the MPPT scheme.

Both control units are integrated into a single algorithm through a cost function that accounts for nonlinear constraints, minimizes system tracking errors, and applies the optimal switching vectors to both converters. Simulation results confirm excellent performance in reference tracking, dynamic response, and robustness against load and wind speed variations. Furthermore, the power carried to the building and the grid exhibits very low THD. Thus, the WECS can autonomously satisfy the building's energy needs, reducing reliance on conventional fossil energy sources.

REFERENCES

[1] Du Parlement européen et du Conseil. (2010). Directive 2010/31/UE du Parlement européen et du Conseil du 19 mai 2010 sur la performance énergétique des bâtiments (refonte).

https://www.legifrance.gouv.fr/jorf/id/JORFTEXT000022388738.
[2] Liserre, M., Cardenas, R., Molinas, M., Rodriguez, J. (2011). Overview of multi-MW wind turbines and wind parks. IEEE Transactions on Industrial Electronics, 58(4): 1081-1095. http://doi.org/10.1109/TIE.2010.2103910
[3] Lakhdara, A., Bahi, T., Izgheche, Y., Henchiri, A. (2025). Improving speed tracking performance of PMSM-driven electric vehicles using a hybrid SMC-MPC approach. Journal Européen des Systèmes Automatisés, 58(9): 1823-1829. https://doi.org/10.18280/jesa.580905
[4] Nikolic, A.B., Rivera, M., Bebic, M., Milosavljevic, S. (2017). Predictive control of a current source rectifier in wind energy conversion system with PMSG. In 2017 IEEE Southern Power Electronics Conference (SPEC), Puerto Varas, Chile, pp. 1-6. http://doi.org/10.1109/SPEC.2017.8333671
[5] Hichem, M., Tahar, B. (2017). Fuzzy monitoring of stator and rotor winding faults for DFIG used in wind energy conversion system. International Journal of Modelling, Identification and Control, 27(1): 49-57. https://doi.org/10.1504/IJMIC.2017.082485
[6] Chub, A., Jalakas, T., Milczarek, A., Kallaste, A., Malinowski, M. (2014). Grid integration issues of PMSG-based residential wind turbines. In 2014 Electric Power Quality and Supply Reliability Conference (PQ), Rakvere, Estonia, pp. 147-154. http://doi.org/10.1109/PQ.2014.6866800
[7] Eftichios, K., Kalaitzakis, K. (2006). Design of a maximum power tracking system for wind-energy-conversion applications. IEEE Transactions on Industrial Electronics, 53(2): 486-494. http://doi.org/10.1109/TIE.2006.870658
[8] Sangeeta, K., Kushwaha, V., Gupta, T.N. (2018). A maximum power point tracking for a PMSG based variable speed wind energy conversion system. In 2018 International Conference on Power Energy, Environment and Intelligent Control (PEEIC), Greater Noida, India, pp. 789-794. http://doi.org/10.1109/PEEIC.2018.8665484
[9] Izgheche, Y., Bahi, T., Lakhdara, A. (2024). Intelligent power management control for hybrid wind solar battery systems connected to micro-grids. Journal Européen des Systèmes Automatisés, 57(4): 1225-1233. https://doi.org/10.18280/jesa.570429
[10] Marmouh, S., Boutoubat, M., Mokrani, L. (2016). MPPT fuzzy logic controller of a wind energy conversion system based on a PMSG. In 2016 8th International Conference on Modelling, Identification and Control (ICMIC), Algiers, Algeria, pp. 296-302. http://doi.org/10.1109/ICMIC.2016.7804126
[11] Gevaert, L.F.M., De Kooning, J.D.M., Vandoorn, T.L., Van de Vyver, J., Vandevelde, L. (2013). Evaluation of the MPPT performance in small wind turbines by estimating the tip-speed ratio. In 2013 48th International Universities' Power Engineering Conference (UPEC), Dublin, Ireland, pp. 1-5. http://doi.org/10.1109/UPEC.2013.6714990
[12] Hassine, I.M.B., Naouar, M.W., Mrabet-Bellaaj, N. (2016). Predictive control strategies for wind turbine system based on permanent magnet synchronous generator. ISA Transactions, 62: 73-80. http://doi.org/10.1016/j.isatra.2015.12.002
[13] Han, B., Lee, H., Yoon, D. (2009). Hardware simulator development for PMSG wind power system. In 2009 IEEE Power & Energy Society General Meeting, Calgary, AB, Canada, pp. 1-6. http://doi.org/10.1109/PES.2009.5275770
[14] Aissaoui, A., Khouidmi, H., Benzouaoui, A., Bessedik, B. (2021). Nonlinear predictive control method for maximizing wind energy extraction of variable speed wind turbines under turbulence. Journal Européen des Systèmes Automatisés, 54(5): 661-670. https://doi.org/10.18280/jesa.540501
[15] Dahbi, A., Hachemi, M., Nait-Said, N., Nait-Said, M.S. (2014). Realization and control of a wind turbine connected to the grid by using PMSG. Energy Conversion and Management, 84: 346-353. http://doi.org/10.1016/j.enconman.2014.03.085
[16] Lekhchine, S., Bahi, T., Soufi, Y. (2013). Direct torque control for double star induction motor. International Journal of Renewable Energy Research, 3(1): 121-125. https://dergipark.org.tr/en/pub/ijrer/article/168280
[17] Tiwari, R., Kumar, K., Ramesh Babu, N., Prabhu, K.R. (2018). Coordinated MPPT and DPC strategies for PMSG based grid connected wind energy conversion system. Energy Procedia, 145: 339-344. http://doi.org/10.1016/j.egypro.2018.04.061
[18] El Mourabit, Y., Derouich, A., El Ghzizal, A., Bouchnaif, J., El Ouanjli, N., Zamzoum, O., Mezioui, K., Bossoufi, B. (2019). Implementation and validation of backstepping control for PMSG wind turbine using dSPACE controller board. Energy Reports, 5: 807-821. https://doi.org/10.1016/j.egyr.2019.06.015
[19] Matraji, I., Al-Durra, A., Errouissi, R. (2018). Design and experimental validation of enhanced adaptive second-order SMC for PMSG-based wind energy conversion system. International Journal of Electrical Power & Energy Systems, 103: 21-30. http://doi.org/10.1016/j.ijepes.2018.05.022
[20] Ayadi, M., Salem, F.B., Derbel, N. (2015). Sliding mode approach for blade pitch angle control wind turbine using PMSG under DTC. In 2015 16th International Conference on Sciences and Techniques of Automatic Control and Computer Engineering (STA), Monastir, Tunisia, pp. 758-762. http://doi.org/10.1109/STA.2015.7505131
[21] Youssef, A.R., Mohamed, E.E.M., Ali, A.I.M. (2018). Model predictive control for grid-tie wind-energy conversion system based PMSG. In 2018 International Conference on Innovative Trends in Computer Engineering (ITCE), Aswan, Egypt, pp. 467-472. http://doi.org/10.1109/ITCE.2018.8316668
[22] Rodriguez, J., Pontt, J., Silva, C., Cortes, P., Ammann, U., Rees, S. (2007). Predictive current control of a voltage source inverter. IEEE Transactions on Industrial Electronics, 54(1): 495-503. http://doi.org/10.1109/TIE.2006.888802
[23] Remache, S.E.I., Cherif, A.Y., Barra, K. (2019). Optimal cascaded predictive control for photovoltaic systems: Application based on predictive emulator. IET Renewable Power Generation, 13(15): 2740-2751. https://doi.org/10.1049/iet-rpg.2019.0068
[24] Matayoshi, H., Howlader, A.M., Datta, M., Senjyu, T. (2018). Control strategy of PMSG based wind energy conversion system under strong wind conditions. Energy

for Sustainable Development, 45: 211-218. http://doi.org/10.1016/j.esd.2018.07.001

[25] Ciupăgeanu, D.A., Lăzăroiu, G., Berbece, V., Tîrşu, M., Galbură, V. (2018). Modeling and control of a low power wind turbine. In 2018 International Conference on Development and Application Systems (DAS), Suceava, Romania, pp. 26-30. http://doi.org/10.1109/DAAS.2018.8396065

[26] Tripathi, S.M., Tiwari, A.N., Singh, D. (2015). Grid-integrated permanent magnet synchronous generator based wind energy conversion systems: A technology review. Renewable and Sustainable Energy Reviews, 51: 1288-1305. http://doi.org/10.1016/j.rser.2015.06.060

[27] Dris, Y., Benhabib, M.C., Meliani, S.M., Dumbrava, V. (2021). Performance analysis of a hybrid farm (photovoltaic system wind turbine) connected to the grid using nine-switches converter. UPB Scientific Bulletin, Series C: Electrical Engineering and Computer Science, 83(3): 207-224. https://www.scientificbulletin.upb.ro/static/pdfs/fulle9f_978201.pdf.

[28] Tahiri, F., Harrouz, A., Dumbrava, V., Badoud, A., Alnatoor, M. (2022). Non-linear controls for robustness investigation of PMSG-based wind turbine. UPB Scientific Bulletin, Series C: Electrical Engineering and Computer Science, 84(2): 377-396. https://www.scientificbulletin.upb.ro/static/pdfs/full98a_253492.pdf.

[29] Shehata, E.G. (2017). A comparative study of current control schemes for a direct-driven PMSG wind energy generation system. Electric Power Systems Research, 143: 197-205. https://doi.org/10.1016/j.epsr.2016.10.039

[30] Shotorbani, A.M., Mohammadi-Ivatloo, B., Wang, L., Marzband, M., Sabahi, M. (2019). Application of finite-time control Lyapunov function in low-power PMSG wind energy conversion systems for sensorless MPPT. International Journal of Electrical Power & Energy Systems, 106: 169-182. http://doi.org/10.1016/j.ijepes.2018.09.039

[31] Belabbas, B., Denai, M., Allaoui, T. (2020). A hierarchical control scheme to improve the stability and energy quality of a hybrid wind/photovoltaic system connected to the electricity grid. UPB Scientific Bulletin, Series C: Electrical Engineering and Computer Science, 82: 307-323. https://www.scientificbulletin.upb.ro/static/pdfs/fullf2a_329239.pdf.

[32] Reangkittakarn, S., Tammaruckwattana, S. (2017). Interconnection inverter control system of PMSG wind power generation. Procedia Computer Science, 111: 406-412. http://doi.org/10.1016/j.procs.2017.06.041

[33] Song, D.R., Yang, J., Dong, M., Joo, Y.H. (2017). Model predictive control with finite control set for variable-speed wind turbines. Energy, 126: 564-572. http://doi.org/10.1016/j.energy.2017.02.149

[34] Araújo, J., Gamboa, P., Chaves, M., Lopes, J. (2019). Predictive optimal control for back to back conversion system for PMSG: Grid interface and power quality assessment. In IECON 2019-45th Annual Conference of the IEEE Industrial Electronics Society, Lisbon, Portugal, pp. 4758-4763. http://doi.org/10.1109/IECON.2019.8926993